

## **Biological and Biomedical Journal**

Journal homepage: https://bbj.journals.ekb.eg



Effect of Azithromycin on the renal cortex of adult male albino rats and the potential protective role of *Annona muricata* (graviola) leaves extract: Histological and immunohistochemical study

#### Dalia El-sayed El-ghazouly

Histology Department, Faculty of Medicine, Menousia University

#### ARTICLE INFO

# **Received**: 26/6/2025 **Revised**: 20/9/2025 **Accepted**:17/10/2025

#### Corresponding author:

Dalia El-sayed El-ghazouly, Ph.D E-mail: daliaelghazouly@yahoo.com Mobile(+2) 01010711153

P-ISSN: 2974-4334 E-ISSN: 2974-4324

DOI:

10.21608/bbj.2025.396070.1112

#### **ABSTRACT**

Azithromycin (AZ) is a highly effective antibiotic used to treat various bacterial infections. However, its use is associated with some serious renal adverse effects. Annona muricata, commonly known as graviola (GRV), is a tropical tree that has been used for its numerous medicinal properties for a long time. This work aims to evaluate the effect of AZ on the renal cortex of rats and the potential protective role of GRV leaves extract. Forty adult male albino rats were equally classified into four groups: Group I (Control), group II (GRV): Received GRV leaves extract (200 mg/kg/day) orally, group III (AZ): Received AZ (30 mg/kg/day) orally, group IV (GRV+AZ): Received GRV and followed by AZ using the same doses of group II and III. For four weeks, the medication was administered once daily. At the end of the experiment, blood and kidney samples were obtained. The AZ-treated group revealed severe alterations in the renal cortex such as degenerated glomeruli, distorted renal tubules with cytoplasmic vacuoles, massive cellular infiltration, and increased collagen deposition. Ultrastructural observations revealed glomerular basement membrane thickening, fusion of podocyte's feet processes, and degenerated mitochondria. A Highly Significant increase in p53-positive cell number, COX-2, and α-SMA immunoreactivity was noticed. Highly significant changes in serum urea, creatinine level, superoxide dismutase activity, and malondialdehyde level were detected. GVR administration with AZ minimized these changes. In conclusion, GVR leaves extract can be a promising protective agent for alleviating AZinduced changes in the renal cortex.

Keywords: Azithromycin, COX-2, Graviola, P53, α-SMA

#### 1. Introduction

Azithromycin (AZ) is a macrolide antibiotic and the only agent in the azalide subclass. It exhibits wide antibacterial action against anaerobic and aerobic bacteria (Hamza et al., 2022). The Food and Drug Administration (FDA) approved AZ to treat sexually transmitted infections and respiratory tract infections (Mansour et al., 2021). It was regarded as a strong oral antibiotic that was usually well tolerated. Its wide range of action, quick oral absorption, once-daily dosage, tissue penetration, and superior tolerability are the main reasons for its popularity (Radwan et al., 2021). The way that AZ works is by

preventing bacteria from synthesizing proteins, which stops them from growing. This gives it broad-spectrum antibacterial properties. It stops mRNA translation by attaching itself to the bacterial ribosome's 50S subunit (Dinos, 2017).

In recent years, AZ was incorporated into the COVID-19 treatment regimen that has been affecting people worldwide since December 2019. It can be taken alone or in conjunction with antimalarial medication hydroxychloroquine (Kashef and Elswaidy, 2022). In March 2020, the French government conducted some research to determine whether AZ and the anti-malarial medication hydroxychloroquine worked well

together to treat COVID-19. All patients cured quickly, and the results revealed significant improvement (Gautret et al., 2020). Early use of AZ in the treatment regimen greatly enhanced clinical results, such as the duration of hospitalization or the requirement for respiratory assistance. AZ can reduce viral penetration inside the cell; moreover, it can increase the immune system's ability to fight off viral infection by enhancing the synthesis of interferon type I and III and genes that recognize viruses (Abd El-Naeem et al., 2022). AZ's antiviral and immunomodulatory properties support its possible effectiveness in treating COVID-19 infection (Rohym et al., 2024). Despite its efficacy and clinically improved results, AZ therapy was linked to some renal negative consequences, like renal failure and acute interstitial nephritis. Based on cohort studies and case reports, these renal alterations were thought to be caused by the impact of the medication and its metabolites on ribosomal function with prolonged presence of these compounds inside tissue (Ismael and Elsamman, 2022).

These days, the world is interested in natural protective extracts that reduce drug side effects and offer new hope for supporting medicine (Gao et al., 2019). The Annonaceae family includes the evergreen fruit tree Annona muricata, known as graviola, which is primarily found in the world's tropical and subtropical regions (Son et al., 2021). In the tropical areas, every part of GRV, including the root, leaves, bark, and fruitseeds, is utilized in natural medicine. It has contributed to its numerous uses in traditional medicine. The leaves have traditionally been used for diabetes, headaches, cystitis, hypertension, liver disorders, insomnia, and as an antispasmodic. Leaves are used to treat skin conditions in tropical Africa (Sabra and Ahmed, 2018). The extract from various GRV parts has a lot of phytoconstituents, including flavonoids (luteolin, rutin, homoorientin, quercetin, daidzein, and tangeretin), glycosides, alkaloids, gallate, epicatechin, coumaric acid, emodin, phenolics, megastigmanes, essential oils, and cyclopeptides (Yang et al., 2015). Additionally, graviola has rich content of annonaceous acetogenin compounds, which exhibit pesticidal, antitumor, anthelmintic, antimalarial, antimicrobial, antifungal, and antiviral effects (Abd El-Monem and Elwakeel, 2020). Because GRV contains strong antioxidants, including polyphenols and flavonoids that protect against the buildup of reactive oxygen species (ROS), recent studies have shown that it can be beneficial in preventing cancer and degenerative diseases like renal diseases (Zeweil et al., 2024). Furthermore, the leaves showed inhibition of pro-inflammatory cytokines, offering defense against both acute and chronic inflammations (Moawad and Elhindawy, 2022). This study intended to explore the effect of AZ on the renal cortex of rats and to assess the potential protective role of A.muricata (graviola) leaves using histological extract and immunohistochemical methods.

#### 2. Materials and Methods

#### **Drugs**

Azithromycin (AZ), a product of Amoun Pharmaceutical Co. El-Obour City, Al Qalyubia, Egypt, available in a tablet form 500 mg with the trade name Xithrone. The drug was given orally after being dissolved in water, 83 ml distilled water was used to dissolve one tablet to get a solution containing 6 mg/ml.

A. muricata leaves extract was purchased from Inkanatural (Lima, Peru), available in a capsule form of 500 mg with the trade name Graviola (GRV). The drug was given orally after being dissolved in water; 12.5 ml of distilled water was used to dissolve one capsule to get a solution with 40 mg/ml.

#### **Animals**

This study utilized forty adults male Wistar albino rats weighing between 170 and 200 grams, obtained and housed in the animal house of the Faculty of Medicine, Menoufia University. The animals were put in suitable, clean plastic cages with mesh wire and acclimatized for one week before the experiment. They were kept under standard conditions of temperature (23  $\pm$  2 °C) and lighting (12 h light/dark cycles). Their normal and healthy circumstances were preserved by strict maintenance of hygiene and care. They were given free access to water and a healthy pellet meal. All animal procedures were achieved in accordance with the guidelines for

the care and use of experimental animals established by the Research Ethical Committee, Faculty of Medicine, Menoufia University, Egypt as well as approved protocols (Approval number: 5/2025 HIST 14).

# **Experimental design:**

The rats were classified into 4 groups. Each of 10 rats. For four weeks, the medication was administered orally once daily. Group I (control group): Rats were subdivided into subgroup Ia and subgroup Ib, each contained 5 rats: Subgroup Ia: Not treated during the entire duration of the experiment. Subgroup Ib: Received 1 ml distilled water orally by gastric tube. Group II (GRV group): Received GRV leaves extract at dose of 200 mg/kg/day orally (Zeweil et al., 2024). Group III (AZ group): Received AZ at a dose of 30 mg/kg/day orally (Usadadia et al., 2020). Group IV (GRV+AZ group): Received GRV leaves extract 1h before AZ using the identical dosages as earlier groups. At the end of the pentobarbital experiment, injections intraperitoneally (35 mg/kg) (Gaertner et al., 2008) were used to anesthetize the rats, after which they were sacrificed and dissected.

## **Biochemical study**

Blood samples were collected twenty-four hours after the final dose for biochemical analysis at the clinical pathology lab of Menoufia University. Blood samples were centrifuged at 3000 rpm for 15 minutes to obtain the serum, then frozen and kept at -20 C until use. For assessment of the renal functions, urea and creatinine levels were spectrophotometrically assessed according to Kessler and Siekmann, (1999) and Chromy et al. (2008). The superoxide dismutase (SOD) activity, and malondialdehyde (MDA) level were determined spectrophotometrically according to Kakkar et al. (1984) and Bhutia et al. (2011).

# Histopathological and immunohistochemistry Investigations

The two kidneys were separated and cleaned by normal saline. Samples were prepared for examination under a light and electron microscope.

#### Light microscopic study

Tissue was put for 3 days in 10% neutralbuffered formalin and then underwent standard processing to produce regular paraffin blocks. Hematoxylin and eosin (H&E) stain was used for usual histological analysis and Masson's trichrome stain was used to detect collagen fibers (Kiernan, 2015). Streptavidin-biotin complex technique (Suvarna et al., 2013a) was used for detection of immunohistochemical studies of p53, cyclooxygenase-2 (COX-2), and Alphasmooth muscle actin (α-SMA). the anti- p53 antibody (catalog number: ab131442, abcam, Cambridge, UK), a rabbit polyclonal antibody, was employed. Positive reaction appeared as nuclear brown coloration. To demonstrate the inflammation, anti-COX-2 antibody, a rabbit polyclonal antibody (catalog number: bs-10411 R, BIOSS, China). Positive reaction appeared as cytoplasmic brown coloration. Marker of smooth muscles and myofibroblasts. Using anti-α-SMA antibody, rabbit polyclonal antibody (catalog number: ab5694, Abcam, Cambridge, UK).

# Transmission electron microscopic study

Specimens from the renal cortex were processed for TEM study according to Suvarna et al. (2013b). The specimens were divided into small pieces (1 mm<sup>3</sup>) and preserved in 2.5% glutaraldehyde for 20 h, then washed with phosphate buffered saline and fixed in 1% osmium tetroxide. Semithin sections (1 µm) were prepared, stained with 1% toluidine blue, and examined under a light microscope for proper orientation. Ultrathin sections (80-90 nm) were cut with an ultramicrotome, stained with uranyl acetate and lead citrate and carried on copper grids to be examined using JOEL (Japan) electron microscope at Tanta University's Faculty of Medicine in Electron Microscopic Unit.

#### **Morphometric measurements**

Area% exhibiting collagen fibers in Masson's trichrome-stained sections at  $\times$  200 magnification, mean number of p53 positive cells, area % of COX-2, and  $\alpha$ -SMA immune-expressions at  $\times$  400 magnification were evaluated. A digital image analysis system (Program Leica Q 500 MC; UK, Cambridge, Leica) was used to take all measurements in the anatomy department of Menoufia University's

Faculty of Medicine. Ten sections, chosen at random from five animals in every group, were utilized for the measurements.

# Statistical analysis

The findings of the biochemical and morphometric analyses have been statistically analyzed utilizing program SPSS, version 17 (IBM Corporation, Somars, NewYork, USA). The outcomes were displayed using the mean ± SEM. The "Tuckey" post hoc test was used after an ANOVA to compare the groups. If a comparison's P value was lower than 0.001, it was deemed highly significant; if it was below 0.05, it was deemed significant; if it was higher than 0.05, it was deemed non-significant (Emsley et al., 2010).

#### 3. Results

There were no recorded deaths during the entire duration of the experiment. Subgroups 1a and 1b didn't exhibit any variations in the histological, immunohistochemical, and morphometric investigations. Also, no significant changes in GRV group (II) compared to control group were detected.

#### Histological study

#### Haematoxylin and Eosin staining

When examining H&E-stained sections of the renal cortex of the control group (I), proximal and distal convoluted tubules and renal corpuscles were found to make up the renal cortex. The renal corpuscle consisted of tuft of capillaries called glomerulus surrounded by Bowman's capsule. Bowman's capsule was formed of inner visceral and outer parietal layers that were separated by Bowman's space. Simple squamous epithelium was found to line the outer parietal layer. Proximal convoluted tubules (PCT) possess narrow lumen and were lined by single layer of pyramidal cells. Their cells possessed a basal rounded nucleus and cytoplasm that was acidophilic. Distal convoluted tubules (DCT) showed wider lumen and were lined by

cubical cells. Their cells had a faint acidophilic cytoplasm and central, rounded nucleus (Fig. 1A). In contrast, the AZ group (III) exhibited severe alterations in the renal cortex. Different levels of glomerular involvement were observed, including dilated congested glomerular capillaries, segmentation of tufts of capillaries and severe degeneration with widened Bowman's space. The renal tubules were markedly damaged and dilated and their lining cells had pyknotic nuclei and cytoplasmic vacuoles. Within the lumens of certain tubules, sloughing necrotic cells were visible. Empty spaces were noticed in the renal cortex. The renal cortex had areas of hemorrhage and dilated congested blood vessels. Additionally, the renal cortex showed signs of acidophilic hyaline exudate and extensive cellular infiltration (Figs. 1B, C, D, E). Sections from group IV (GRV+AZ) showed that the renal tubules' histological structure was almost normal, except for few pyknotic shrunken nuclei and some dilatation of lumen. Additionally, the glomeruli seemed almost normal, except for mild glomerular capillary congestion and Bowman's space widening. Little cellular infiltration and slight hemorrhage were observed in between tubules (Fig. 1F).

#### Masson's trichrome staining

Sections of renal cortex of control group (I) displayed minimal amount of collagen fibers surrounding the renal tubules and corpuscles and in between the glomeruler capillaries (Fig. 2A). The AZ group (III), on the other hand, showed an overabundance of collagen fibers deposited around dilated congested blood vessels, surrounding the renal tubules and corpuscles and in between the glomerular capillaries (Fig. 2B). Sections from group IV (GRV+AZ) exhibited mild amount of collagen fibers around mildly dilated blood vessels, around renal tubules and corpuscles and in between the glomerular capillaries (Fig. 2C).

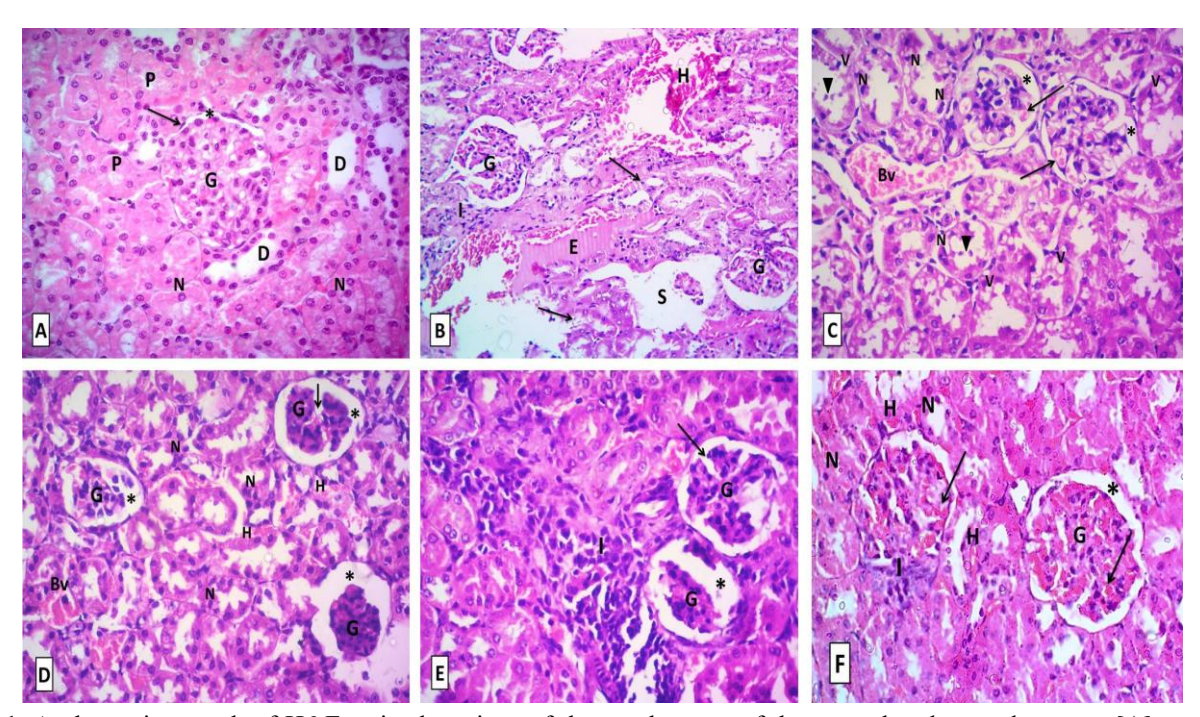
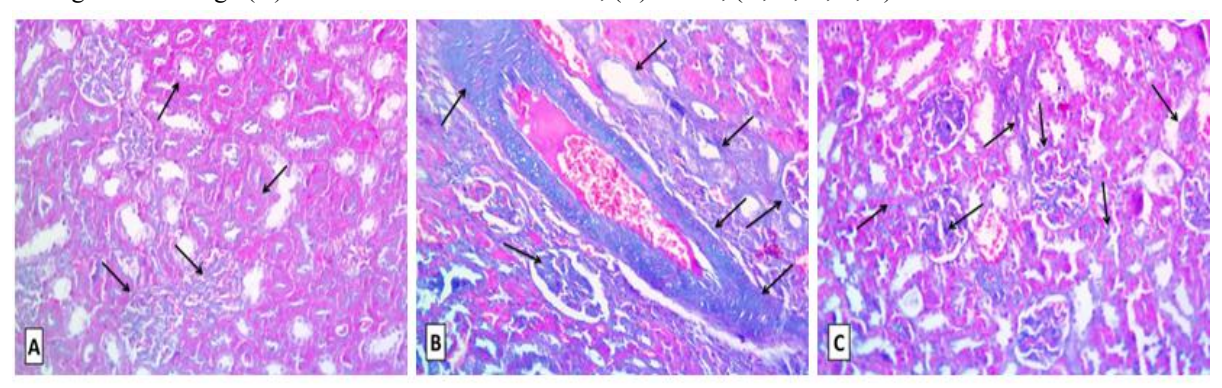


Fig.1. A photomicrograph of H&E-stained sections of the renal cortex of the control and treated groups. [A]: control group (I) showing a renal corpuscle which is composed of the glomerulus (G) surrounded by Bowman's space (\*) that lined by simple squamous epithelium (arrow), proximal convoluted tubules (P) are lined by pyramidal cells with a narrow lumen. Distal convoluted tubules (D) are lined by cubical cells with a wider lumen. Presence of acidophilic cytoplasm and vesicular nuclei (N) of the tubular cells. [B]: AZ group (III) showing marked distortion of glomeruli (G) and renal tubules (arrows) with empty spaces (S) in between. Areas of hemorrhage (H), cellular infiltration (I) and acidophilic hyaline exudate (E) are observed. [C]: AZ group (III) showing disorganized glomeruli; dilated congested glomerular capillaries (arrows) and widened Bowman's space (\*). Dilated congested blood vessel (Bv) is observed. The distortion of renal tubules is noticed with cytoplasmic vacuoles (V) and pyknotic shrunken nuclei (N) in their lining cells. Notice: sloughing necrotic cells (arrow heads) in the dilated lumen of tubules. [D]: AZ group (III) showing markedly degenerated glomeruli (G) with widening of Bowman's space (\*). Segmentation of tufts of glomerular capillaries (arrow) is noticed. Dilated congested blood vessels (By) and areas of hemorrhage (H) are seen in between the tubules. Notice: distortion of renal tubules with pyknotic shrunken nuclei (N). [E]: AZ group (III) massive cellular infiltration (I) within the renal cortex. Markedly degenerated glomeruli (G) are observed with widening of Bowman's space (\*). Segmentation of tufts of glomerular capillaries (arrow) is noticed. [F]: GRV+AZ group (IV) showing normal appearance of renal tubules except for few pyknotic shrunken nuclei (N) and some dilatation of lumen. The glomerulus (G) appears nearly normal except for mild congestion of glomeruler capillaries (arrows) and widening of Bowman's space (\*). Notice: little cellular infiltration (I) and slight hemorrhage (H) in between the tubules. H&E, (B) X 200, (A, C, D, E, F) X 400



**Fig. 2.** A photomicrograph of Masson's trichrome-stained sections of the renal cortex of the control and treated groups. [A]: control group (I) showing minimal amounts of collagen fibers surrounding the renal tubules and corpuscles and in between the glomeruler capillaries (arrows). [B]: AZ group (III) showing marked amount of collagen fibers around a dilated congested blood vessel, around the renal tubules and corpuscles and in between the glomeruler capillaries (arrows). [C]: GRV+AZ group (IV) showing mild amount of collagen fibers around mildly dilated blood vessels, around renal tubules and corpuscles and in between the glomerular capillaries (arrows). Masson's trichrome, (A, B, C) X 200.

# Immunohistochemical study P53 immunostaining

Sections of renal cortex of control group (I) revealed negative nuclear immunoreaction for p53 in almost tubular cells and cells of the renal corpuscles. Very few tubular cells exhibited weak reaction for P53 (Fig. 3A). In contrast, AZ group (III) exhibited strong positive brown nuclear immunoreaction for p53 in numerous tubular cells and cells of the renal corpuscles (Fig. 3B). Regarding group IV (GRV+AZ), it exhibited moderate to strong positive brown

nuclear p53 immunoreaction in some tubular cells and cells of the renal corpuscle (Fig. 3C).

#### **COX-2** immunostaining

Sections of renal cortex of control group (I) demonstrated weak to mild positive cytoplasmic immunoreaction for COX-2 in the renal corpuscles and the renal tubules (Fig. 4A). In contrast, AZ group (III) exhibited strong positive cytoplasmic COX-2 immunoreaction in the renal corpuscles and tubules (Fig. 4B). While group IV (GRV+AZ) displayed mild to moderate positive cytoplasmic COX-2 immunoreaction in the renal corpuscles the renal tubules (Fig. 4C).

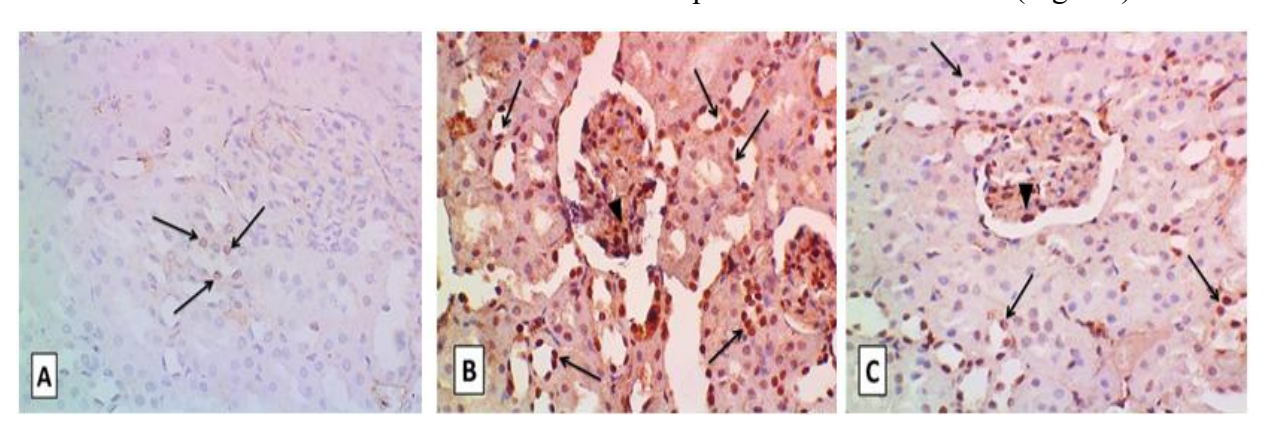


**Fig. 3.** A photomicrograph of P53-stained sections of the renal cortex of the control and treated groups. **[A]:** control group (I) showing negative nuclear immunoreaction for p53 in almost tubular cells and cells of the renal corpuscle. Weak positive brown nuclear immunoreaction for p53 is noticed in very few tubular cells (arrows). **[B]:** AZ group (III) showing strong positive brown nuclear immunoreaction for p53 in numerous tubular cells (arrows) and cells of the renal corpuscle (arrowhead). **[C]:** GRV+AZ group (IV) showing moderate to strong positive brown nuclear immunoreaction for p53 in some tubular cells (arrows) and cells of the renal corpuscle (arrowhead). P53 and Hematoxylin as a counter stain, (A, B, C) X 400

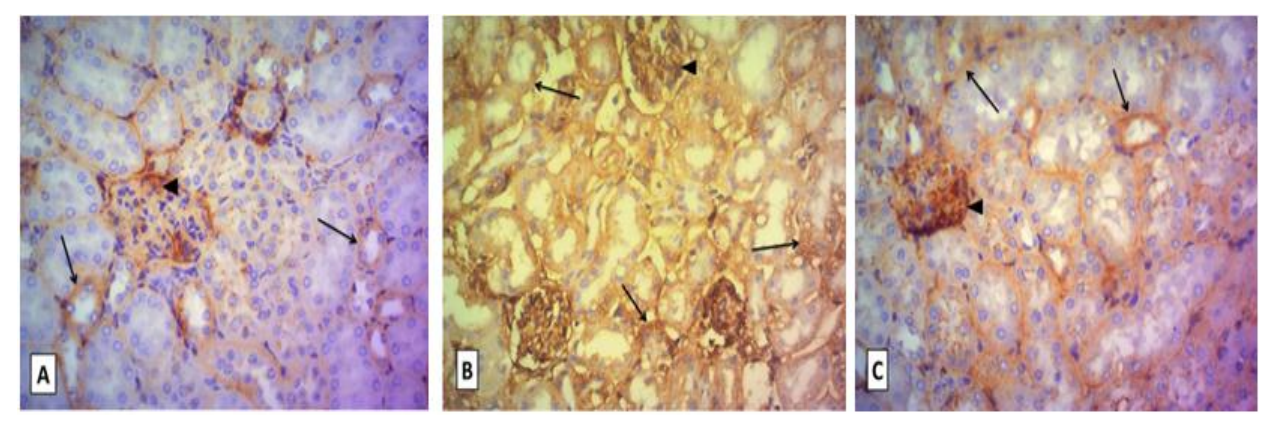


**Fig. 4.** A photomicrograph of COX-2-stained sections of the renal cortex of the control and treated groups. **[A]**: control group (I) showing weak to mild positive cytoplasmic immunoreaction for COX-2 in the renal corpuscle (arrowhead) and the renal tubules (arrows). **[B]**: AZ group (III) showing strong positive cytoplasmic immunoreaction for COX-2 in the renal corpuscle (arrow head) and the renal tubules (arrows). **[C]**: GRV+AZ group (IV) showing mild to moderate positive cytoplasmic immunoreaction for COX-2 in the renal corpuscle (arrow head) and the renal tubules (arrows). COX-2 and Hematoxylin as a counter stain, (A, B, C) X 400

# α-SMA immunostaining

Sections of renal cortex of control group (I) demonstrated negative  $\alpha$ -SMA immunoreaction in the renal corpuscles and around tubules Positive α-SMA immunoreaction was observed in the wall of the blood vessels (Fig. 5A). AZ group (III) exhibited widespread positive α-SMA immunoreaction in the renal corpuscles and in the interstitial around tubules. Also, positive α-SMA immunoreaction was observed in the wall of the dilated blood vessels and in elongated cells around the vessels (Figs. 5B, 5C). Regarding group IV (GRV+AZ), it exhibited scarce positive α-SMA immunoreaction in the renal corpuscles and in the interstitial around tubules. Positive α-SMA immunoreaction was observed in the wall of blood vessels (Fig. 5D).

## Transmission electron microscopic results

Electron microscopy findings of the control group (I) showed typical ultrastructure of the renal cortex. The podocytes appeared normal with euchromatic nucleus containing nucleolus. The cell body of podocytes gave major processes (primary processes) from which secondary processes arose and terminated by feet-like expansions on the capillary wall. Podocyte foot processes were regularly space out enclosing in between filtration slits closed by diaphragm. The glomerular basement membrane had regular diameter. The glomerular blood capillaries were lined by endothelium with open fenestrae (Figs. 6A, 6B).

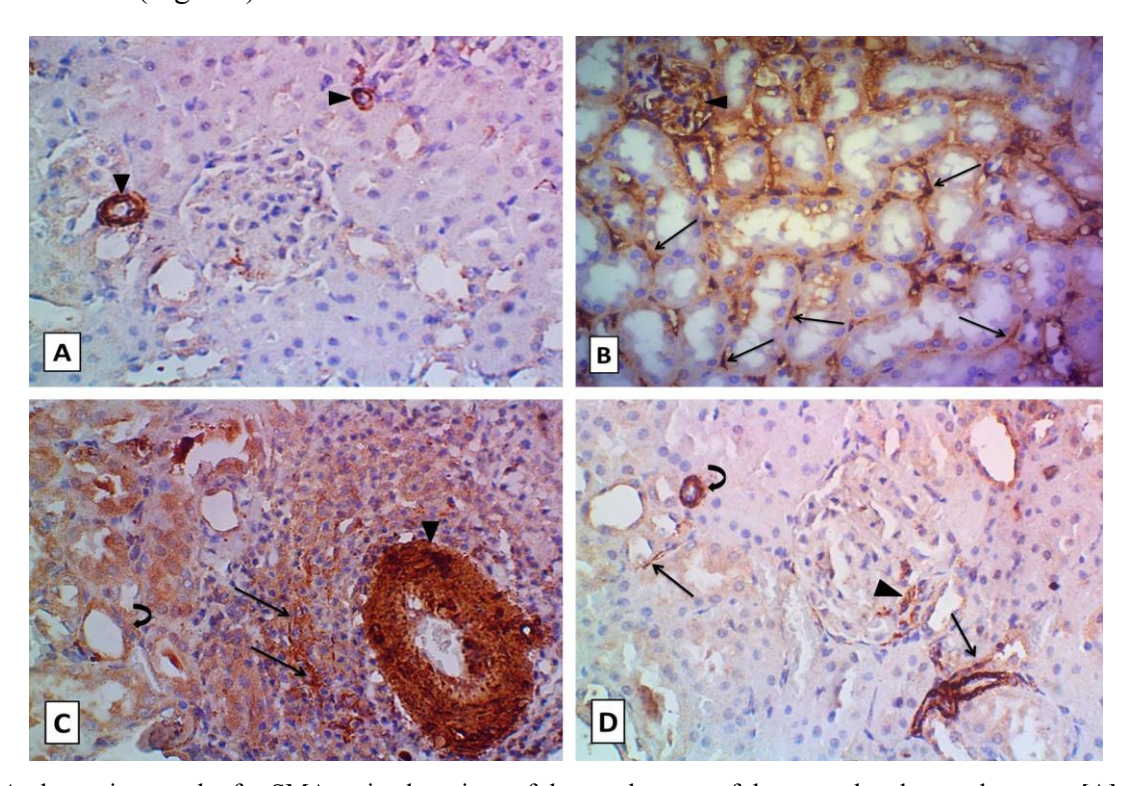


**Fig. 5.** A photomicrograph of α-SMA-stained sections of the renal cortex of the control and treated groups. **[A]:** control group (I) showing positive α-SMA immunoreaction in the wall of the blood vessels (arrowheads). Negative α-SMA immunoreaction is observed in the renal corpuscle and around tubules. **[B]:** AZ group (III) showing widespread positive α-SMA immunoreaction in the renal corpuscle (arrowhead) and in the interstitium around tubules (arrows). **[C]:** AZ group (III) showing positive α-SMA immunoreaction in the wall of the dilated blood vessel (arrowhead) and in elongated cells around the vessel (arrows). Positive α-SMA reaction is observed in the interstitium around tubules (curved arrow). **[D]:** GRV+AZ group (IV) showing scarce positive α-SMA immunoreaction in the renal corpuscle (arrowhead) and in the interstitium around tubules (arrows). Positive α-SMA immunoreaction is observed in the wall of the blood vessel (curved arrow). α-SMA and Hematoxylin as a counter stain, (A, B, C, D) X 400.

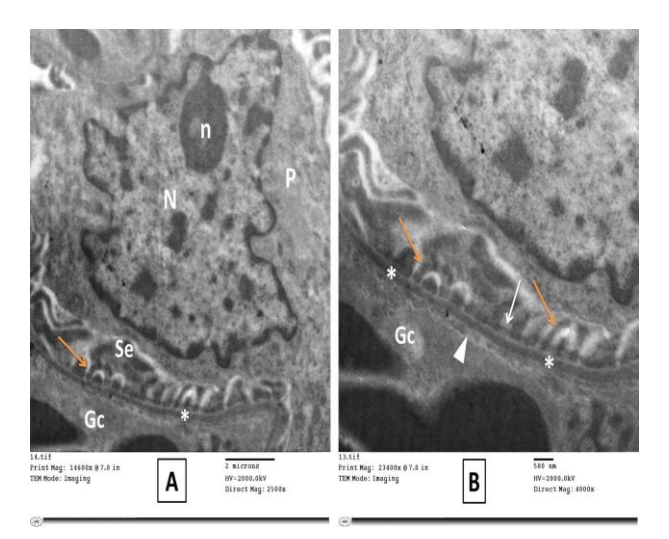


Fig. 6. An electron micrograph from control group (I). [A]: showing a podocyte (P) with euchromatic nucleus (N) containing nucleolus (n). Secondary (minor) processes (Se) terminated by feet-like expansions (orange arrow) on the capillary wall are seen. Notice: a glomerular blood capillary (Gc) and the basement membrane (\*). [B]: a higher magnification of [A] showing glomerular basement membrane (\*) which is smooth and of regular diameter. Regularly space out podocyte foot processes (orange arrows) enclosing in between filtration slits closed by diaphragm (white arrow) are observed. Notice: a glomerular blood capillary (Gc) lined by endothelium with open fenestrae (white arrowhead). A X 2500, B X 4000

convoluted tubule (PCT) Proximal appeared with a central oval euchromatic nucleus, basal elongated vertically oriented mitochondria, lysosomes and apical long densely packed microvilli. The cells rested on regular thin basement membrane (Fig. 7A). Distal convoluted tubule (DCT) cells had central oval euchromatic nucleus and basal plasma membrane enfolding's with palisade arrangement of numerous longitudinally oriented mitochondria. Few or no microvilli were projecting into the lumen. The cells rested on a thin regular basement membrane with intact intercellular junction in between (Fig. 7B).

In contrast, the AZ group (III) exhibited remarkable ultrastructure changes involving the renal corpuscles, proximal and distal convoluted tubules. The podocytes shrunken had heterochromatic nucleus and exhibited effacement and fusion of their secondary feet processes. The glomerular basement membrane revealed apparent moderate to marked thickening (Figs. 8A, 8B).

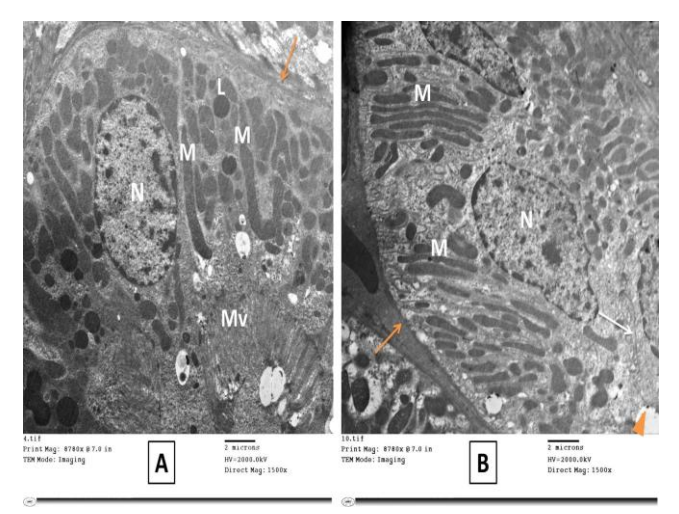


Fig. 7. An electron micrograph from control group (I). [A]: showing a PCT cell with a central oval euchromatic nucleus (N), basal elongated vertically oriented mitochondria (M) and apical long closely packed microvilli (Mv). Lysosomes (L) are observed. Notice: The cell rests on a thin regular basement membrane (orange arrow). [B]: showing a DCT cell having a central oval euchromatic nucleus (N) and basal plasma membrane enfolding's with palisade arrangement of numerous longitudinally oriented mitochondria (M). Few or no microvilli (orange arrowhead) are projecting into the lumen. The cell rests on a thin regular basement membrane (orange arrow). Intact intercellular junction is noticed (white arrow). (A, B) X 1500

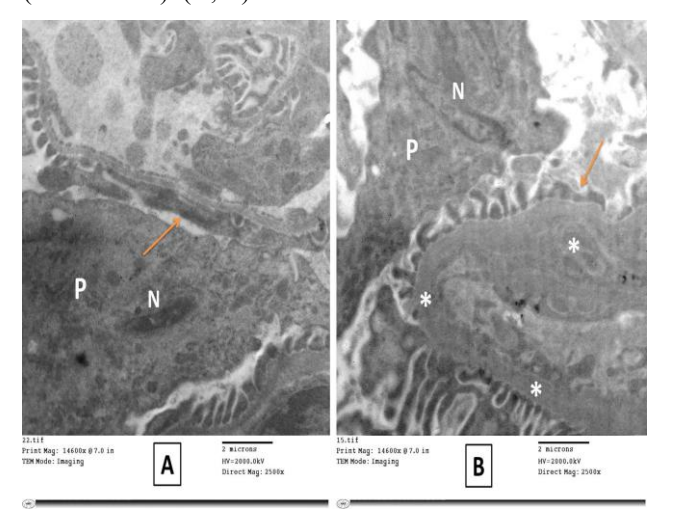


Fig. 8. An electron micrograph from AZ group (III). [A]: showing a podocyte (P) with shrunken heterochromatic nucleus (N). Effacement and fusion of secondary feet processes is observed (orang arrow). [B]: showing apparent moderate to marked thickening of the glomerular basement membrane (\*). Focal effacement and fusion of feet processes is observed (orange arrow). Notice: a podocyte (P) with shrunken heterochromatic nucleus (N) (A, B) X 2500.

Some PCT cells exhibited partial loss of apical microvilli and their cytoplasm appeared rarefied with swollen and broken mitochondria and multiple vacuoles, most probably degenerated mitochondria (Fig. 9A). Other PCT cells had shrunken heterochromatic nucleus and abnormal mitochondrial arrangement with irregularity of basement membrane (Fig. 9B).

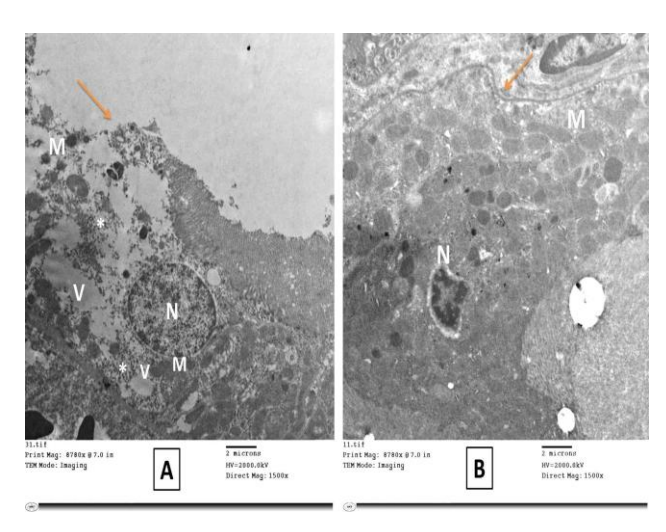
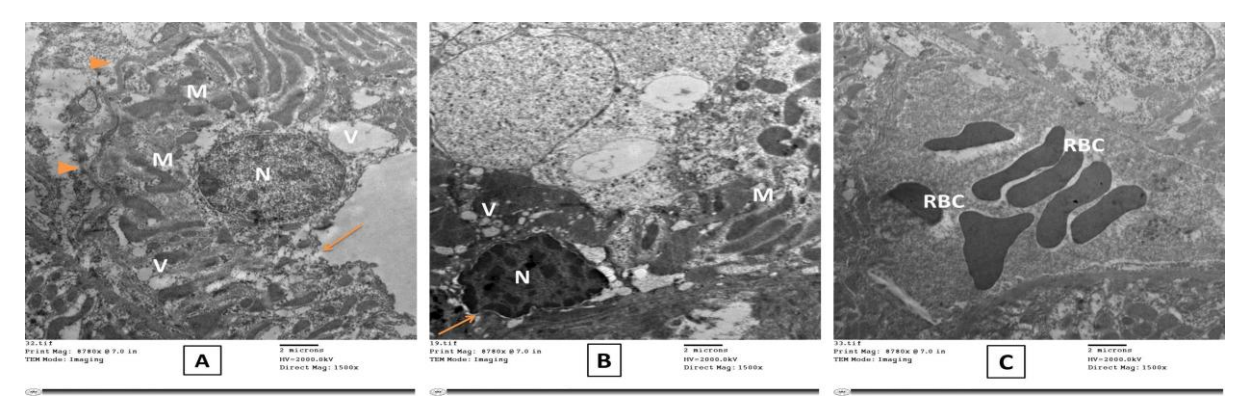


Fig. 9. An electron micrograph from AZ group (III). [A]: showing a PCT cell with a central rounded euchromatic nucleus (N) and partial loss of apical microvilli (orange arrow). The cytoplasm appears rarefied (\*) with multiple vacuoles (V), most probably degenerated mitochondria. Some mitochondria (M) appear swollen and broken. [B]: showing a PCT cell with a shrunken heterochromatic nucleus (N) and abnormal mitochondrial arrangement (M). Notice: irregularity of basement membrane (orange arrow) (A, B) X 1500.

The cells of DCT appeared with irregular heterochromatic nucleus and disrupted apical surface. Their cytoplasm showed multiple degenerated vacuoles. most probably mitochondria. There was loss of palisade arrangement of the mitochondria. Some cells rested on irregular basement membrane (Figs. 10A, 10B). The intersitium between the tubules showed extravasated red blood cells (Fig. 10C). Interestingly, group IV (GRV+AZ) exhibited much preservation of the ultrastructure of the renal cortex. Podocytes showed euchromatic nucleus with few areas of fusion and effacement of their feet processes. The glomerular basement membrane was regular with apparent normal thickness. The glomerular blood capillaries were lined by endothelium with open fenestrae (Fig. 11A). There was more or less intact structure of PCT cells exhibiting euchromatic nucleus with prominent nucleolus, basal mitochondria, lysosomes and intact apical microvilli and few vacuoles. Few cells appeared with shrunken heterochromatic nucleus (Figs. 11B, 11C). Also, there was more or less intact structure of DCT cells exhibiting euchromatic nuclei and normal arrangement of mitochondria between the basal infoldings. The cells rested on a thin basement membrane and revealed intact intercellular junction in between (Fig. 11D).

#### **Biochemical investigations**

Compared to the control group, Group III (AZ group) showed a highly significant increase in serum urea levels. Similarly, Group IV (GRV+AZ) exhibited a highly significant elevation in the same parameter relative to the control group. Comparing group IV to group III, there was highly significant drop-in group IV (Table 1, Fig. 12-A). Serum creatinine level of group III (AZ group) revealed highly significant rise relative to control group. Similarly, Group IV (GRV+AZ) demonstrated highly significant increase in the identical measure relative to control group. Comparing group IV to group III, there was highly significant reduction in group IV (Table 1, Fig. 12-B). Compared to the control group, group III (AZ group) revealed highly significant decline in serum SOD activity. Group IV (GRV+AZ) exhibited significant reduction in the identical measure relative to control group. Comparing group IV to group III, there was highly significant rise in group IV (Table 1, Figure 12-C). while, MDA level of group III (AZ group) revealed highly significant rise relative to control group. Group ΙV (GRV+AZ)demonstrated highly significant increase in the identical measure relative to control group. Comparing group IV to group III, there was highly significant reduction in group IV (Table 1, Fig. 12-D).



**Fig. 10.** An electron micrograph from AZ group (III). [A]: showing a DCT cell with a heterochromatic nucleus (N) and disrupted apical surface (orange arrow). The cytoplasm shows multiple vacuoles (V), most probably degenerated mitochondria. Loss of the palisade arrangement of the mitochondria (M) is noticed. Notice: irregularity of basement membrane (orange arrowheads). [B]: showing a DCT cell with an irregular heterochromatic nucleus (N) and dilated perinuclear space (orange arrow). The cytoplasm shows multiple vacuoles (V) with loss of the palisade arrangement of the mitochondria (M). [C]: showing extravasated red blood cells (RBC) in the intersitium between the tubules. (A, B, C) X 1500

**Table 1.** The biochemical and statistical results in the control and experimental groups

	Group I	Group II	Group III	Group IV	P-value		
					(P1 > 0.05) *		
Serum urea	22.21	21.91	40.09	29.84	$(P2 < 0.001)^{***}$		
(mg/dl)	$\pm 2.19$	$\pm  2.05$	$\pm  3.19$	$\pm 2.31$	(P3< 0.001) ***		
					(P4< 0.001) ***		
C					(P1 > 0.05)*		
Serum creatinine	0.52	0.53	1.38	0.88	$(P2 < 0.001)^{***}$		
(mg/dl)	$\pm 0.03$	$\pm  0.03$	$\pm 0.12$	$\pm  0.06$	$(P3 < 0.001)^{***}$		
					$(P4 < 0.001)^{***}$		
					(P1 > 0.05) *		
Serum SOD	33.98	34.33	20.65	29.52	$(P2 < 0.001)^{***}$		
(U/ml)	$\pm  2.05$	$\pm 1.74$	$\pm  2.54$	$\pm 2.34$	$(P3 < 0.05)^{**}$		
					$(P4 < 0.001)^{***}$		
					(P1 > 0.05) *		
Serum MDA	5.03	4.84	17.12	8.43	$(P2 < 0.001)^{***}$		
(nmol/ml)	$\pm 0.63$	$\pm 0.52$	$\pm  2.09$	$\pm 1.36$	$(P3 < 0.001)^{***}$		
					$(P4 < 0.001)^{***}$		

Data are presented as Mean  $\pm$  SD, **P1:** Group I vs. Group II; **P2:** Group I vs. Group III; **P3:** Group I vs. Group IV; **P4:** Group III vs. Group IV. Non-significant \* (P > 0.05), Significant\*\* (P < 0.05), Highly significant\*\*\* (P < 0.001).

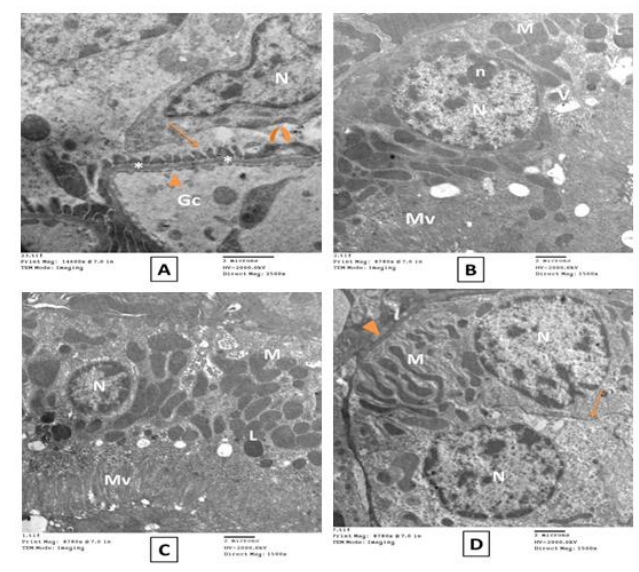


Fig. 11. An electron micrograph from GRV+AZ group (IV). [A]: showing podocyte with euchromatic nucleus (N) and secondary foot processes (orange arrow), few of them show fusion and effacement (curved arrow). Regular basement membrane with apparent normal thickness (\*) is seen. Notice: a glomerular blood capillary (Gc) lined by endothelium with open fenestrae (orange arrowhead). [B]: showing more or less intact structure of PCT cell. Euchromatic nucleus (N) with prominent nucleolus (n), basal mitochondria (M), lysosomes (L) and intact apical microvilli (Mv) are seen. Few vacuoles (V) are noticed. [C]: showing more or less intact structure of PCT cell. Shrunken heterochromatic nucleus (N) is observed. Basal mitochondria (M), lysosomes (L) and intact apical microvilli (Mv) are seen. [D]: showing more or less intact structure of two DCT cells. Euchromatic nuclei (N) and normal arrangement of mitochondria (M) between the basal infoldings are observed. Intact intercellular junction is observed (orange arrow). The cells rest on a thin basement membrane (orange arrowhead). A X 2500, (B, C, D) X 1500

#### Morphometric results

## The Area% % of collagen fibers

When compared to the control group, group III (AZ group) exhibited a highly significant increase in mean area percentage of collagen fibers. Group IV (GRV+AZ) demonstrated significant rise in the identical measure relative to control group. Group IV experienced a highly significant decline in comparison to group III (Table 2, Fig. 13-A).

# The mean number of p53

Group III (AZ group) demonstrated highly significant increase in number of apoptotic p53 positive cells relative to control group. Group IV (GRV+AZ) demonstrated a highly significant increase in the identical measure relative to control group. When compared group IV to group III, there was highly significant reduction in group IV (Table 2, Figure 13-B).

# Area% of COX-2 immunoexpression

Group III (AZ group) exhibited a highly significant rise in mean area percentage of COX-2 immunoexpression relative to control group. Group IV (GRV+AZ) demonstrated highly significant rise in the identical measure relative to the control group. When comparing group IV to group III, there was highly significant decline in group IV (Table 2, Figure 13-C).

# Area% of α-SMA immunoexpression

Group III (AZ group) demonstrated a highly significant rise in the mean area percentage of  $\alpha$ -SMA immunoexpression in comparison with the control. Group IV (GRV+AZ) demonstrated a significant rise in the identical measure relative to the control group. When comparing group IV to group III, there was a highly significant decline in group IV. (Table 2, Fig. 13-D).

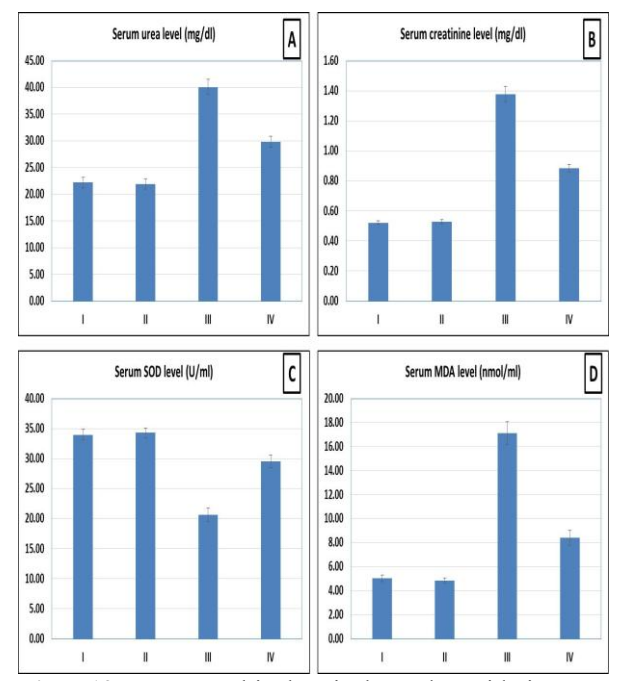


**Fig. 12.** Serum biochemical and oxidative stress parameters across experimental groups. Data are presented as mean ± SD **(A)** Serum urea level (mg/dl). **(B)** Serum creatinine level (mg/dl). **(C)** Serum SOD level (U/ml). **(D)** Serum MDA level (nmol/ml). **I:** control gp, **II:** GRV gp, **III:** AZ gp, **IV:** GRV+AZ gp

**Table 2.** The morphometric and statistical results in the control and experimental groups

	1 8 1						
	Group I	Group II	Group III	Group IV	P-value		
Area percentage of collagen fibers	6.07 ± 0.89	6.11 ± 1.12	27.12 ± 4.50	9.58 ± 1.84	(P1 > 0.05) * (P2 < 0.001) *** (P3 < 0.05) ** (P4 < 0.001) ***		
Number of p53 positive cells	8.80 ± 2.86	9.20 ± 3.42	108.60 ± 15.24	68.80 ± 8.76	(P1 > 0.05) * (P2 < 0.001) *** (P3 < 0.001) *** (P4 < 0.001) ***		
Area percentage of COX-2	5.21 ± 1.5	4.89 ± 1.19	28.84 ± 3.07	10.26 ± 1.72	(P1 > 0.05) * (P2 < 0.001) *** (P3 < 0.001) *** (P4 < 0.001) ***		
Area percentage of α-SMA immunoexpression	2.41 ± 1.16	2.12 ± 1.03	23.59 ± 4.52	5.99 ± 1.15	(P1 > 0.05) * (P2 < 0.001) *** (P3 < 0.05)** (P4 < 0.001) ***		

Data are presented as Mean  $\pm$  SD, P1: Group I vs. Group II, P2:Group I vs. Group III, P3: Group I vs. Group IV, P4: Group III vs. Group IV, Non-significant \* (P > 0.05), Significant\*\* (P < 0.05), Highly significant\*\*\* (P < 0.001).

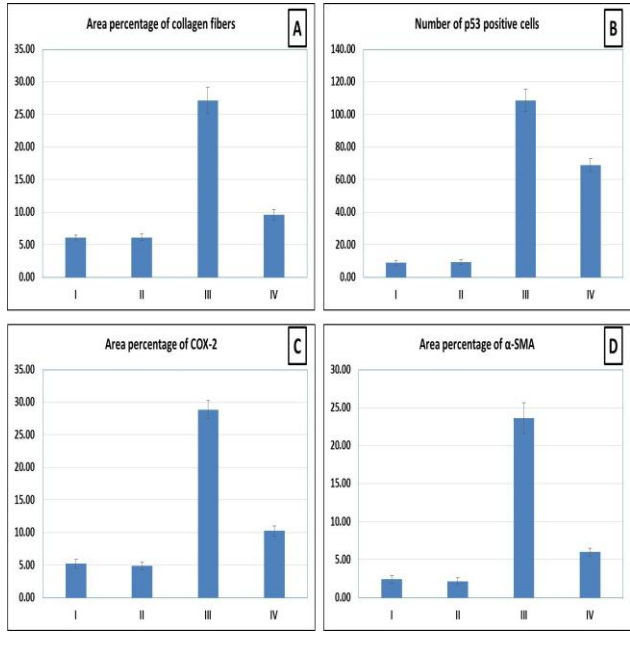


**Fig. 13.** Morphometric and statistical results in the control and experimental groups showing: (A) The mean area percentage of collagen fibers.(B) The mean number of p53 positive cells.(C)The mean area percentage of COX-2.(D) The mean area percentage of α-SMA. **I:** control gp, **II:** GRV gp, **III:** AZ gp, **IV:** GRV+AZ gp

#### 4. Discussion

Azithromycin is a broad-spectrum macrolide that is frequently used to treat a variety of diseases, particularly pneumonia. Additionally, it is one of the medications used in the COVID-19 therapy program (Kim et al., 2020). Azithromycin's lipophilia gives it ability to spread freely in body fluid and tissue and so can exert the antibacterial effect. However, numerous studies indicate that it is cytotoxic to the liver, heart and kidney that showed some side effects as renal failure and acute interstitial nephritis (Atli et al., 2015; Usadadia et al., 2020; Ismael and Elsamman, 2022).

The well-known tropical plant A. muricata leaves, known as soursop or graviola, has long been used to treat variety of conditions, including pain, infections, respiratory conditions, fever, hypertension, cancer and diabetes (Mutakin et al., 2022). It is utilized for its anticancer, antiviral, antibacterial. anti-fungal, antimalarial, antioxidant, analgesic, anxiolytic, hypotensive, hypoglycemic gastroprotective, hepatoprotective, immunomodulatory, and anti-inflammatory properties (Zeweil et al., 2024). However, few reports are available on its protective impact against kidney damage.

Consequently, this work was designed to explore azithromycin effect on renal cortex of rats and to evaluate the potential protective role of *A. muricata* (graviola) leaves extract histologically and immunohistochemically.

In the current study, H&E-stained sections of the renal cortex of azithromycin treated group displayed various histopathological changes. There were segmentation of tufts of capillaries and dilated congested glomerular capillaries in some glomeruli, while other glomeruli displayed sever degeneration with widened Bowman's space. The renal tubules were markedly distorted and dilated, and the lining cells had pyknotic nuclei and cytoplasmic vacuoles. There were empty spaces, hemorrhage, congested blood vessels and massive cellular infiltration in renal cortex. These light microscopic findings were in agreement with those of prior studies (Usadadia et al., 2020; Ismael and Elsamman, 2022). The electron microscopic results confirmed light microscopic results as there were effacement and fusion of the secondary feet processes of podocytes as well as thickening of glomerular basement membranes. The renal tubular cells revealed cytoplasmic vacuolations probably degenerated mitochondria), swollen and broken mitochondria, partial loss of apical microvilli in PCT, disrupted apical surface of **DCT** cells together with shrunken heterochromatic nuclei.

Biochemical outcomes concerning serum levels of urea and creatinine of AZ group supported the histopathological changes as there was highly significant rise in their levels relative to the control. Similar findings were detected in an earlier work (Usadadia et al., 2020) where the authors suggested the impairment of renal function as a result of azithromycin. They stated that serum levels of the metabolic waste products urea and creatinine, which are readily filtered by the kidneys' glomeruli, are frequently used to screen for renal disorders. They added that high urea and creatinine level in the blood is a sign of aberrant renal function.

The histopathological findings of AZ group could be attributed to the production of extremely reactive free radicals as a result of the drug's oxidative hazard, which interfered with normal cellular function of the kidney as has been

previously reported by some authors (Olayinka and Ore, 2014; Usadadia et al., 2020). It is known that even after a single dose, AZ can stay in the tissues for up to a month, and its blood serum concentration can be at least 100 times higher than that of tissues (Ismael and Elsamman, 2022). Additionally, Salimi et al. (2016) attributed the generation of reactive oxygen species (ROS) by AZsuppressed to mitochondrial respiration, which is followed by oxidative damage to DNA. Moreover, Kashef and Elswaidy (2022) stated that the disruption of the antioxidant defense system and the rise in ROS production are the causes of azithromycin's damaging effects.

This interpretation was supported by biochemical outcomes of the current study regarding serum SOD and MDA levels, which revealed evidence for oxidative stress. The azithromycin-treated group exhibited a highly significant reduction in SOD (antioxidant enzyme) serum level and a highly significant increase in MDA (lipid peroxidation marker) serum level. Similar results were detected in prior studies on azithromycin-induced toxicity (Atli et al., 2015; Radwan et al., 2021; Rohym et al., 2024). Atli et al. (2015) where the authors reported that MDA, SOD, catalase glutathione levels are biomarkers used to evaluate the oxidative status, and these markers exhibited significant changes as a result of azithromycin, reflecting the occurrence of oxidative stress in rats. They added that increased oxidative stress in organs such as the heart, and liver can cause structural, kidneys, biochemical, and functional harm. Radwan et al., (2021) reported that free radicals and ROS produced by azithromycin may change the expression and functions of antioxidant enzymes. They added that increased MDA level by azithromycin indicated an increase in lipid peroxidation which could be connected to a decrease in antioxidant systems (enzymatic and non-enzymatic) leading to accelerated lipid oxidation.

In the current study, glomerular basement membrane thickening observed in AZ group may be attributed to the glomerular capillaries' large surface area, which makes them vulnerable to large amounts of harmful substances in the blood as has been previously reported by Ali et al., (2021). Also, effacement and fusion of podocyte's feet processes may be caused by ROS overproduction, which resulted in cytoskeletal changes such as actin disaggregation (Hegazy et al., 2023).

In the current study, the AZ group revealed cytoplasmic vacuoles and heterochromatic nuclei in the tubular cells and podocytes, which are features of apoptosis as has been previously reported (Farag and Sabry, 2020). Such findings were supported by the immunohistochemical results for p53, which recorded a highly significant increase of apoptotic p53-positive cells of the AZ group. The p53 is an apoptotic protein that antagonizes Bcl-(an anti-apoptotic protein) and causes permeability in the mitochondrial membrane, which triggers apoptosis (Nur et al., 2022). This suggests that oxidative stress triggered by azithromycin caused apoptosis in the renal cortex. Outcomes of this study agreed with those of previous works (Ismael and Elsamman, 2022; Kashef and Elswaidy, 2022; Rohym et al., 2024) using immunohistochemical studies for caspase-3 and Bcl-2 and found that azithromycin increases ROS generation, which leads to apoptosis. Additionally, Salimi et al. (2016) reported that AZ causes the mitochondrial membrane to become more permeable, which causes the mitochondria to swell, release cytochrome c, and trigger apoptosis. The results of the current study supported such explanation as there were swollen and broken mitochondria as well as multiple vacuoles, most probably degenerated mitochondria in the AZ group. It was suggested by some authors (El-Hawwary and Sarhan, 2017) that degenerated mitochondria may be represented as cytoplasmic vacuoles and they added that mitochondria are very liable to harmful substances and when they are destroyed, cell metabolism fails with additional damage to the cell.

The current investigation found several indicators of inflammation, including massive cellular infiltration, dilated congested blood vessels along with hemorrhage and acidophilic hyaline exudate. Similar findings were described in a previous study (Ismael and Elsamman, 2022) which reported that AZ intensifies the

inflammatory response because it boosts proinflammatory cytokines as TNF- $\alpha$  and IL-1. Chen et al., (2017) stated that free radicals could cause inflammatory responses through cytokines that regulate the migration of leukocytes into sick areas. It is well recognized that TNF-α draws leukocytes to inflammatory areas and promotes the production of additional reactive species. Furthermore, several inflammatory and apoptotic mediators that cause structural damage may be produced by TNF-α (Abd El-kader, 2020). In the current study, these inflammatory signs were consistent with the immunohistochemical results of the AZ group that revealed a highly significant the area percent of COX-2 in immunoexpression. COX-2 expression triggered by inflammatory stimuli or mediators. According to studies, the macula densa is where COX-2 expression is normally detected in the renal cortex. The reason for this is that under normal circumstances, COX-2 is present in the macula densa in small but measurable quantities because it is the source of prostaglandins derived from the macula densa that mediate the production of renin by juxtaglomerular cells Aboulkhair, (Ismail and 2019). inflammatory cytokines like TNF-α and ILs cause COX-2 expression to be up-regulated. Furthermore, it is induced by the production of ROS and prostanoids, which are inflammatory mediators that intensify inflammatory reaction (Wang et al., 2018). Increased cytokine production from different cells raises COX2 expression, an enzyme that produces a range of inflammatory mediators, including prostaglandins and leukotrienes (Sarbishegi et al., 2016).

In the present study, the renal cortex of AZ treated group exhibited overabundance of collagen fibers deposited around dilated congested blood vessels, renal tubules and corpuscles and in between the glomeruler capillaries reflecting fibrosis and such finding was validated by statistical analysis which exhibited highly significant rise in collagen area percent relative to control group. Similar finding was detected in prior study (Ismael and Elsamman, 2022) on effect of AZ on the Kidney and the authors owed the collagen deposition to the increased release of free radicals, which

caused oxidative injury to cellular proteins, lipids and DNA. Moreover, Elkomy et al., (2018) reported that AZ damaged the kidney's tubular lining epithelium, causing degeneration and necrosis, and generated fibrosis in between the atrophied renal tubules. Abd El-kader, (2020) explained the occurrence of fibrosis by the transformation of fibroblasts into myofibroblasts that produce a large amount of collagen. Such explanation was confirmed in the current study by the immunohistochemical results of the AZ group, which revealed a highly significant rise in the area percent of α-SMA (marker of myofibroblasts) compared to the control. Such a result matched with the results of prior studies on azithromycin toxicity (Abd El-kader, 2020; Kashef and Elswaidy, 2022), which clarified that α-SMA immunohistochemical detection can be used determine the existence myofibroblasts, which displayed features of both fibroblasts and smooth muscle cells. Yaseen et al. (2019) stated that protease inhibitors released by myofibroblasts may lead to increased production and decreased turnover of extracellular matrix proteins, leading to fibrosis development.

In group IV (GRV+AZ), A. muricata (graviola) leaves extract was given with azithromycin to assess its possible role in alleviating the renal cortex changes induced by azithromycin. Graviola (GRV) exerted a protective effect on the renal cortex as shown by the histological and immunohistochemical findings. The histological structure of the renal cortex was largely preserved. However, there were heterochromatic nuclei in a few tubular cells, mild congestion of glomeruler capillaries, widened Bowman's space, little cellular infiltration, and slight hemorrhage in between tubules. Biochemical and morphometric results of this group confirmed such findings. The levels of creatinine and urea in the blood were significantly reduced relative to the AZ group. All these findings matched with earlier works (Sabra and Ahmed, 2018; Zeweil et al., 2024) in which the authors detected renoprotective effect by GRV against renal cortex damage, and they attributed this effect to the antioxidant and anti-inflammatory features of GRV. Graviola's antioxidant capability could be attributed to the leaves' polyphenol content. Leaves of A. muricata were shown in prior

studies (Yang et al., 2015, Oliveira et al., 2017) to contain strong antioxidants as kaempferol, quercetin-glucoside, quercetin, and rutin. These substances have the capacity to scavenge free radicals, donate electrons, or decrease hydrogen in addition to producing stable antioxidantderived radicals (Zeweil et al., 2024). Jiménez-Osorio et al. (2015) reported that Flavonoids and other phenolic acids found in GRV have been shown to either activate ROS reduction capability that is linked to activation of antioxidant genes, or limit the oxidation of cell macromolecules through the radical scavenging capabilities. Moreover, Zeweil et al. (2024) stated that the presence of acetogenins in GRV gives it strong antioxidant properties, which can be essential for scavenging reactive oxygen species.

The antioxidant capability of GRV was confirmed in the current study, as there was a highly significant rise in serum SOD level and drop in serum MDA level in group IV(AZ+GRV) compared to the AZ group. Similar outcomes were obtained by previous studies (Sabra and Ahmed, 2018; Abd El-Monem and Elwakeel, 2020; Zeweil et al., 2024) on the protective impact of GRV. Also, there was a highly significant decrease of apoptotic p53-positive cells in group IV (GRV+AZ) compared to the AZ group. A similar finding was recorded in a prior study (Shukry et al., 2020) where the authors detected that GRV decreased higher levels of Bax, caspase 3, and P53 and attributed this to its antioxidant activity, which leads to an increase in Bcl2 expression and hence prevents DNA fragmentation, cytochrome C release, mitochondrial permeability.

Regarding the anti-inflammatory activity of GRV, It was determined that GRV extract suppressed both COX-1 and COX-2 and decreased inflammatory cytokines (IL-6, IL-8) (Rady et al., 2018; Hong et al., 2021). Moreover, Helal and Abd Elhameed, (2021) proposed that GRV plays a critical function in reducing inflammatory reaction in renal tissues by blocking proinflammatory cytokines and COX-2. These conclusions were supported by data from the current investigation, where GRV+AZ group exhibited highly significant drop in level of COX-2 compared to the AZ group. Zeweil et

al. (2024) reported that anti-inflammatory compounds (saponins, alkaloids, tannins, and flavonoids) in graviola extract may inhibit prostaglandin synthesis, hence maintaining normal levels of IL1 $\beta$  and TNF- $\alpha$  expression.

In the current study, group IV (GRV+AZ) demonstrated a highly significant drop in the area percent of collagen and  $\alpha$ -SMA relative to the AZ group. This was compatible with a prior study (Al-Medhtiy et al., 2022) where the authors reported that graviola resisted liver fibrosis by downregulating  $\alpha$ -SMA reactivity as a result of reducing ROS production.

Conclusion: These findings provided evidence that azithromycin can induce renal cortex damage in rats manifested by biochemical abnormalities, histological, and immunohistochemical alterations. *A.muricata* (graviola) leaves extract was able to minimize azithromycin-induced changes. These outcomes indicate that graviola can be an effective protective agent for alleviating azithromycin-induced changes owing to its antioxidant and anti-inflammatory effects. So, azithromycin should be used cautiously, and co-administration of graviola is highly recommended.

#### 5. Reference

Abd El-kader M, 2020. Evaluation of azithromycin-induced cardiotoxicity in male albino rats and the possible protective role of *Nigella sativa* oil. Egyptian Journal of Histology, 43(2): 465-476.

Abd El-Monem DD, Elwakeel SH, 2020. Protective Effect of Graviola (Annona muricata) Leaves Extract Against Cadmium-Induced Testicular Toxicity In Male Albino Rats. Egyptian Academic Journal of Biological Sciences, B. Zoology, 12(1): 139-154.

Abd El-Naeem AF, Abouelella AMA, Baset AS, 2022. Evaluation of Effect of Azithromycin on The Heart of Adult Male Albino Rats and The Possible Protective role of VIT.C (Histological and Immune-histochemical Study). SVU- International Journal of Medical Sciences, 5(2): 518-532.

Ali AF, Ghoneim NS, Salama R, 2021. Light and electron microscopic study on the effect of

- Gibberellic acid on the renal cortex of adult male albino rats and the possible protective role of Coenzyme Q10. Egyptian Journal of Histology, 44(2): 368-383.
- Al-Medhtiy MH, Jabbar AA, Shareef SH, Ibrahim IAA, Alzahrani AR, Abdulla MA, 2022. Histopathological Evaluation of *Annona muricata* in TAA-Induced Liver Injury in Rats. Processes, 10(8):1613.
- Atli O, Ilgin S, Altuntas H, Burukoglu D, 2015. Evaluation of azithromycin induced cardiotoxicity in rats. Int J Clin Exp Med. 8(3): 3681-90. PMID: 26064263; PMCID: PMC4443097.
- Bhutia Y, Ghosh A, Sherpa ML, Pal R, Mohanta PK, 2011. Serum malondialdehyde level: Surrogate stress marker in the Sikkimese diabetics. J Nat Sci Biol Med. 2(1):107-12. doi: 10.4103/0976-9668.82309. PMID: 22470243; PMCID: PMC3312689.
- Chen L, Deng H, Cui H, Fang J, Zuo Z, Deng J, Li Y, Wang X, Zhao L, 2017. Inflammatory responses and inflammation-associated diseases in organs. Oncotarget. 9(6):7204-7218. doi: 10.18632/oncotarget.23208. PMID: 29467962; PMCID: PMC5805548.
- Chromy V, Rozkosna K, Sedlak P, 2008. Determination of serum creatinine by Jaffe method and how to calibrate to eliminate matrix interference problems. Clin. Chem. laboratory Med. 46, 1127–1133.
- Dinos GP, 2017. The macrolide antibiotic renaissance. Br J Pharmacol. 174(18): 2967-2983. doi: 10.1111/bph.13936. Epub 2017 Aug 10. PMID: 28664582; PMCID: PMC5573421.
- El-Hawwary A, Sarhan N, 2017. Does Olive Oil Attenuate Ciprofloxacin-Induced Renal Cortical Toxicity? Light and Electron Microscopic Study. Egyptian Journal of Histology, 40(2): 253-264.
- Elkomy A, Kandeil AM, Abo- Salem M, Hassan WA, Aboubakr M, Elhemiely AA, 2018. Effect of azithromycin on fetal development in rats. International Journal of Pharmacology and Toxicology, 6 (1)18-23.

- Emsley R, Dunn G, White IR, 2010. Mediation and moderation of treatment effects in randomized controlled trials of complex interventions. Stat Methods Med Res. 19: 237-270.
- Farag EA, Sabry MM, 2020. Intermittent Fasting Attenuates Apoptosis, Modulates Autophagy and Preserves Telocytes in Doxorubicin Induced Cardiotoxicity in Albino Rats: A Histological Study. Egyptian Journal of Histology, 43(3): 663-683.
- Gaertner DJ, Hallman TM, Hankenson FC, Batchelder MA, 2008. Anesthesia and analgesia for laboratory rodents. In: Fish, R.E., Danneman, P.J., Brown, M., Karas, A.Z. (Eds.), Anesthesia and Analgesia in Laboratory Animals, 2<sup>nd</sup> ed. Academic Press, London (UK), 239–297. Hardback ISBN: 9780123738981. eBook ISBN: 9780080559834.
- Gao W, Wang W, Liu G, Zhang J, Yang J, Deng Z, 2019. Allicin attenuated chronic social defeat stress induced depressive-like behaviors through suppression of NLRP3 inflammasome. Metab Brain Dis. 34(1):319-29. doi: 10.1007/s11011-018-0342-z. Epub 2018 Dec 4. PMID: 30515710.
- Gautret P, Lagier JC, Parola P, Hoang VT, Meddeb L, Mailhe M, et al., 2020. Hydroxychloroquine and azithromycin as a treatment of COVID-19: results of an openlabel non-randomized clinical trial. International journal of antimicrobial agents, 56(1):105949.
- Hamza RZ, Alaryani FS, Omara F, Said MAA, El-Aziz SAA, El-Sheikh SM, 2022. Ascorbic Acid Ameliorates Cardiac and Hepatic Toxicity Induced by Azithromycin-Etoricoxib Drug Interaction. Curr Issues Mol Biol. 44(6):2529-2541. PMID: 35735613; PMCID: PMC9222074.
- Hegazy K, Elswaidy N, Kassab A, Elbakary N, 2023. The Effect of Energy Drinks and Their Withdrawal on the Renal Cortex of Adult Male Albino Rats. Histological, Ultrastructural and Morphometric Study. Egyptian Journal of Histology, 46(3): 1282-1295.

- Helal MG, Abd Elhameed AG, 2021. Graviola mitigates acetic acid—induced ulcerative colitis in rats: insight on apoptosis andWnt/Hh signaling crosstalk. Environ. Sci. Pollut. Res. 28: 29615–29628.
- Hong GU, Choi M, Chung MH, Ro JY, 2021. Anti-inflammatory effects of graviola stem bark extracts on the testosterone-induced benign prostatic hyperplasia model in rats. Food Suppl Biomater Health, 1(2): e18.
- Ismael ZM and Elsamman WN, 2022. Evaluation of the Effects of Azithromycin on the Kidney of Adult Albino Rats and the Possible Protective Role of Vitamin C Using Histological and Immuno-Histochemical Studies. SVU-International Journal of Medical Sciences, 5(2): 484-500.
- Ismail D, Aboulkhair A, 2019. The Effect of Aliskiren on Renal Cortical Ischemia/Reperfusion Injury in Albino Rats: A Histological and Immunohistochemical Study. Egyptian Journal of Histology, 42(4): 838-848.
- Jiménez-Osorio AS, González-Reyes S, Pedraza-Chaverri J, 2015. Natural Nrf2 activators in diabetes. Clin Chim Acta. 448:182-192. doi: 10.1016/j.cca.2015.07.009. Epub 2015 Jul 9. PMID: 26165427.
- Kakkar P, Das B, Viswanathan PN, 1984. A modified spectrophotometric assay of superoxide dismutase. Indian J Biochem Biophys. 21(2):130-132. PMID: 6490072.
- Kashef S, Elswaidy N, 2022. 'The Possible Role of Allicin in Ameliorating Azithromycin Induced Cardiotoxicity in Adult Male Albino Rat: A Histological and Immunohistochemical Study'. Egyptian Journal of Histology, 45(3): 863-874.
- Kessler A, Siekmann L, 1999. Measurement of urea in human serum by isotope dilution mass spectrometry: a reference procedure. Clin. Chem. 45: 1523–1529.
- Kiernan JA, 2015. Histological and histochemical methods; theory and practice. 5th ed Oxford, UK: Butterworth Heinemann, 238–310. ISBN 9781907904325

- Kim YS, Lee SY, Yoon JW, Kim D, Yu S, Kim JS, Kim JH, 2020. Cardiotoxicity induced by the combination therapy of chloroquine and azithromycin in human embryonic stem cell-derived cardiomyocytes. BMB Rep. 53(10):545-550. PMCID: PMC7607154
- Mansour BS, Salem NA, Abdel Kader G, Abdel-Alrahman G, Mahmoud OM, 2021. Protective effect of Rosuvastatin on Azithromycin induced cardiotoxicity in a rat model. Life Sciences, 269: 119099. ISSN 0024-3205,
- Moawad AA, Elhindawy MM, 2022. The Possible Protective Effect of Graviola Extract on Salivary Gland Against Cytotoxicity During Cisplatin Treatment (Histological, Biochemical and Immunohistochemical Study). Egyptian Journal of Histology, 45(2): 588-596.
- Mutakin M, Fauziati R, Fadhilah FN, Zuhrotun A, Amalia R, Hadisaputri YE, 2022. Pharmacological activities of soursop (*Annona muricata* Lin.). Molecules, 27(4), 1201.
- Nur G, Caylak E, Kilicle PA, Sandayuk S, Celebi OO, 2022. Immunohistochemical distribution of Bcl-2 and p53 apoptotic markers in acetamiprid-induced nephrotoxicity. Open Med (Wars). 17(1):1788-1796PMID: 36457797; PMCID: PMC9679552
- Olayinka ET, Ore A, 2014. Influence of azithromycin treatment on hepatic lipid peroxidation and antioxidant defence systems of rats. British Journal of Pharmaceutical Research, 4(2):240-256.
- Oliveira AP, Sa I, Pereira DM, Goncalves RF, Andrade PB, Valentao P, 2017. Exploratory studies on the in vitro anti-inflammatory potential of two herbal teas (*Annona muricata* L. And jasminum grandiflorum L.), and relation with their phenolic composition. Chem. Biodivers. 14 (6): e1700002.
- Radwan D, Hussin M, Mahmoud A, 2021. 'Antioxidant Approach of *Nigella Sativa*, Vit C and Silymarin for amelioration of Azithromycin induced Hepatotoxicity: Histological, Immunohistochemical and

- Biochemical study', Egyptian Society of Clinical Toxicology Journal, 9(2), pp. 29-45.
- Rady I, Bloch MB, Chamcheu RCN, Banang Mbeumi S, Anwar MR, Mohamed H, et al., 2018. Anticancer properties of graviola (*Annona muricata*): a comprehensive mechanistic review. Oxidative Med. Cell. Longev. 1826170.
- Rohym HH, Hemeda MS, Elsayed AM, Farrag MS, Elsayed HA, Ezzat AA, Ibrahim MA, Makloph M, 2024. Interleukin-10 levels in azithromycin-induced cardiac damage and the protective role of combined selenium and vitamin E treatment. Toxicol Rep. 14:101860. PMID: 39758799; PMCID: PMC11697843.
- Sabra HA, Ahmed NM, 2018. Reno- protective Effect of Graviola (*Annona Muricata*) Leaves Against Lead Acetate Toxicity on experimental Albino Rats. *Biochemistry Letters*, 14(1): 1-13.
- Salimi A, Eybagi S, Seydi E, Naserzadeh P, Kazerouni NP, Pourahmad J, 2016. Toxicity of macrolide antibiotics on isolated heart mitochondria: a justification for their cardiotoxic adverse effect. Xenobiotica. 46(1):82-93. PMID: 26068526.
- Sarbishegi M, Khajavi O, Arab MR, 2016. *Withania coagulans* extract induces cell apoptosis and inhibits COX-2 expression in a rat model of benign prostatic hyperplasia. Nephro-Urology Mon. 8 (5), e39284.
- Shukry M, El-Shehawi AM, El-Kholy WM, Elsisy RA, Hamoda HS, Tohamy HG, Abumandour MM, Farrag FA, 2020. Ameliorative Effect of Graviola (*Annona muricata*) on Mono Sodium Glutamate-Induced Hepatic Injury in Rats: Antioxidant, Apoptotic, Anti-inflammatory, Lipogenesis Markers, and Histopathological Studies. Animals. 10(11):1996.
- Son Y, Lee H, Son SY, Lee CH, Kim SY and Lim Y, 2021. Ameliorative Effect of *Annona muricata* (Graviola) Extract on Hyperglycemia Induced Hepatic Damage in

- Type 2 Diabetic Mice. Antioxidants, 10: 1546.
- Suvarna SK, Layton C, Bancroft JD, 2013a. Immunohistochemical techniques. In: Bancroft's Theory and Practice of Histological Techniques, 7th ed., Churchill Livingstone Elsevier, London. pp: 387-418. ISBN: 978-0-7020-4226-3
- Suvarna SK, Layton C, Bancroft JD, 2013b. Transmission electron microscopy. In: Bancroft's Theory and Practice of Histological Techniques, 7<sup>th</sup> ed., Elsevier Churchill Livingstone, London. pp: 493-508. ISBN: 978-0-7020-4226-3
- Usadadia SV, Patel JM, Vihol PD, and Urkude AP, 2020. Protective Effect of Quercetin on Azithromycin Induced Hepatotoxicity and Nephrotoxicity in Wistar Rats. Int. J. Curr. Microbiol. App. Sci. 9 (9): 2926-2934.
- Wang Z, Han Q, Guo YL, Liu XH, Qiu T, 2018. Effect of ozone oxidative preconditioning on inflammation and oxidative stress injury in rat model of renal transplantation. Acta Cir Bras. 33(3):238-249.
- Yang C, Gundala SR, Mukkavilli R, Vangala S, Reid MD, Aneja R, 2015. Synergistic interactions among flavonoids and acetogenins in Graviola (*Annona muricata*) leaves confer protection against prostate cancer. Carcinogenesis, 36(6): 656-665. PMCID: PMC4566098.
- Yaseen A, Asker S, Omar N, Abd El Fattah A, 2019. N-Acetylcysteine Mitigates Histopathological and Ultrastructural Alterations Induced by Chronic Usage of Acetaminophen in the Rat Renal Cortex. Egyptian Journal of Histology, 42(1): 162-177.
- Zeweil MM, Khafaga AF, Mahmoud SF, Wasef L, Saleh H, Elrehim AMA, Bassuoni NF, Alwaili MA, Saeedi NH, Ghoneim HA, 2024. *Annona muricata* L. extract restores renal function, oxidative stress, immunohistochemical structure, and gene expression of TNF-α, IL-β1, and CYP2E1 in the kidney of DMBAintoxicated rats. Front. Pharmacol. 15:1348145.